AD-A166 628 A CANDIDATE MESOSCALE NUMERICAL CLOUD/PRECIPITATION MODEL(U) AIR FORCE GEOPHYSICS LAB HANSCOM AFB MA D RIDGE ET AL. 10 OCT 85 AFGL-TR-85-0252 1/1

UNCLASSIFIED F/G 4/2 NL

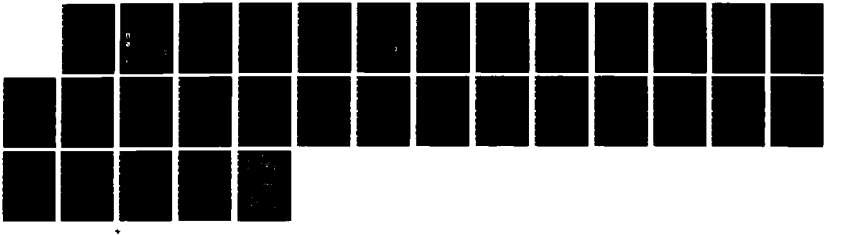

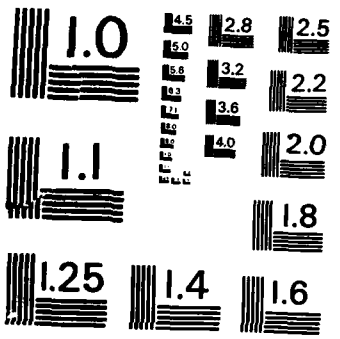

(12)

AFGL-TR-85-0252
ENVIRONMENTAL RESEARCH PAPERS, NO. 931

A Candidate Mesoscale Numerical Cloud/Precipitation Model

DANIEL RIDGE
GEORGE MODICA
ARTHUR JACKSON

10 October 1985

Approved for public release; distribution unlimited.

ATMOSPHERIC SCIENCES DIVISION PROJECT 6670
AIR FORCE GEOPHYSICS LABORATORY
HANSCOM AFB, MA 01731

This technical report has been reviewed and is approved for publication.

FOR THE COMMANDER

H. Stuart Muench

H. STUART MUENCH, Acting Chief
Atmospheric Prediction Branch

Robert A. McClatchey

ROBERT A. McCLATCHEY, Director
Atmospheric Sciences Division

This document has been reviewed by the ESD Public Affairs Office (PA) and is releasable to the National Technical Information Service (NTIS).

Qualified requestors may obtain additional copies from the Defense Technical Information Center. All others should apply to the National Technical Information Service.

If your address has changed, or if you wish to be removed from the mailing list, or if the addressee is no longer employed by your organization, please notify AFGL/DAA, Hanscom AFB, MA 01731. This will assist us in maintaining a current mailing list.

UNCLASSIFIED
SECURITY CLASSIFICATION OF THIS PAGE

AD-A166628

REPORT DOCUMENTATION PAGE

1a. REPORT SECURITY CLASSIFICATION Unclassified	1b. RESTRICTIVE MARKINGS
2a. SECURITY CLASSIFICATION AUTHORITY	3. DISTRIBUTION/AVAILABILITY OF REPORT Approved for public release; distribution unlimited.
2b. DECLASSIFICATION/DOWNGRADING SCHEDULE	
4. PERFORMING ORGANIZATION REPORT NUMBER(S) AFGL-TR-85-0252 ERP, No. 931	5. MONITORING ORGANIZATION REPORT NUMBER(S)
6a. NAME OF PERFORMING ORGANIZATION Air Force Geophysics Laboratory 6b. OFFICE SYMBOL (If applicable) LYP	7a. NAME OF MONITORING ORGANIZATION
6c. ADDRESS (City, State and ZIP Code) Hanscom AFB Massachusetts 01731	7b. ADDRESS (City, State and ZIP Code)
8a. NAME OF FUNDING/SPONSORING ORGANIZATION 8b. OFFICE SYMBOL (If applicable)	9. PROCUREMENT INSTRUMENT IDENTIFICATION NUMBER
8c. ADDRESS (City, State and ZIP Code)	10. SOURCE OF FUNDING NOS. PROGRAM ELEMENT NO. 62101F; PROJECT NO. 6670; TASK NO. 10; WORK UNIT NO. 15

11. TITLE (Include Security Classification)
A Candidate Mesoscale Numerical Cloud/Precipitation Model

12. PERSONAL AUTHOR(S)
Ridge, Daniel, Modica, George, and Jackson, Arthur

13a. TYPE OF REPORT	13b. TIME COVERED	14. DATE OF REPORT (Yr., Mo., Day)	15. PAGE COUNT
Scientific, Final	FROM 9/84 TO 9/85	1985 October 10	30

16. SUPPLEMENTARY NOTATION

17 COSATI CODES			18. SUBJECT TERMS (Continue on reverse if necessary and identify by block number)
FIELD	GROUP	SUB GR	Short Range Forecasting; Mesoscale Modeling; Cloud Forecasting; Precipitation Forecasting; Advanced Weather Distribution System

19. ABSTRACT (Continue on reverse if necessary and identify by block number)

A numerical mesoscale forecast model was selected for potential use by the Air Force in an operational mode, either in a nested configuration, or as a stand-alone model in a base-weather station. The model was developed at the National Oceanographic and Atmospheric Association's (NOAA) Environmental Research Laboratory (ERL), and many of its numerical and meteorological features are described in this report. Two versions are specified: the first under development at NOAA/ERL and another at AFGL (the NOAA/AFGL model). A baseline test of the latter model revealed several problems. The initialization scheme computed initial fields of mass and momentum that failed to mutually adjust after several hours of integration. Subsequent techniques designed to improve the initial conditions appeared to be a step in the right direction. The nonmeteorological gravity-inertia (GI) wave noise evident in most of the forecast fields appeared to result from poor treatment of the variables at the lateral boundaries.

20. DISTRIBUTION/AVAILABILITY OF ABSTRACT UNCLASSIFIED/UNLIMITED ☒ SAME AS RPT ☐ DTIC USERS ☐	21. ABSTRACT SECURITY CLASSIFICATION Unclassified

22a. NAME OF RESPONSIBLE INDIVIDUAL	22b. TELEPHONE NUMBER (Include Area Code)	22c. OFFICE SYMBOL
George Modica	(617) 861-2956	AFGL/LYP

DD FORM 1473, 83 APR EDITION OF 1 JAN 73 IS OBSOLETE

UNCLASSIFIED
SECURITY CLASSIFICATION OF THIS PAGE

Contents

Illustrations

Illustrations

Tables

A Candidate Mesoscale Numerical Cloud/Precipitation Model

1. INTRODUCTION

The United States Air Force is proceeding with a program called the Automated Weather Distribution System (AWDS) in order to modernize base-weather operations of the Air Weather Service through the use of advanced computers and peripheral equipment. This modernization generally will result in efficient and accurate analyses and forecasts of weather systems. In particular, the primary objectives[1] for AWDS are to provide: (1) operational capability for better detection and transmission of critical weather elements; (2) modern display (e.g., CRT) and dissemination of weather observations; (3) a modular system to allow selective combinations of components; and (4) the capability for expansion and incorporation of new display and sensing techniques. In addition, this modernization program will require that AWS stations have the capability to produce automated, numerical forecasts of relevant weather in the zero to 12-h period and for spatial domains ≤ 400 km (meso-beta or "theater" scale). The motivation for the last requirement is the desire to employ objective numerical weather prediction techniques that produce deterministic mesoscale forecasts rather than

(Received for publication 9 October 1985)

1. Air Weather Service (1984) Capabilities Master Plan (CMP) 1984-1985, Headquarters AWS, Scott AFB, Ill.

relying solely on subjective inference from the present system of synoptic-scale guidance, climatology, terrain, and meteorological observations. However, adequate numerical treatment of the dynamic processes that occur on these scales has not yet been realized.

Improvement in mesoscale forecast skill is inhibited by problems in four principal areas.[2] The first area concerns numerical and practical difficulties associated with realistic treatment of lateral and lower boundary conditions in the model. The second is the introduction of significant error in the analyzed initial conditions for the model due to inadequate spatial and temporal resolution of initial upper-air data from the present observational network. The third area is the difficulty stemming from the parameterization in the model of the sub-grid scale physical processes. The fourth problem area is the inherent limit in the predictability of smaller-scale circulations.

The Air Force Geophysics Laboratory (AFGL) has initiated a program to develop predictive, sub-synoptic scale regional models specifically designed to provide 1- to 2-h forecasts of clouds and precipitation. The program at AFGL is intended to select, test, and evaluate a model (or models) that ultimately could be used in two operational modes: (1) by nesting within a larger-scale model, or (2) on a stand-alone basis in a base-weather station, mini-computer environment. The model[3] selected for these studies was developed at the National Oceanographic and Atmospheric Administration (NOAA). It will be described in Section 2.

While much of the development effort of the model (both nested and stand-alone modes) was being carried out by contractors at the NOAA Environmental Research Laboratory,[4] AFGL scientists concluded a baseline test for a preliminary assessment of its capabilities, computer requirements, and possible weaknesses. This technical report will describe the NOAA model, the problems and weaknesses discovered during the baseline test, and a series of suggested remedies to solve these problems.

---

2. Anthes, R.A. (1983) Regional models of the atmosphere in middle latitudes, Mon. Wea. Rev. III:1306-1335.

3. Nickerson, E.C. (1979) On the numerical simulation of airflow and clouds over mountainous terrain, Beit. zur Physik der Atmos. 52:161-177.

4. Nickerson, E.C., Richard, E., Rosset, R., and Smith, D. (1985) On the numerical simulation of clouds, rain, and airflow over the Vosges and Black Forest Mountains: A meso-β model with parameterized microphysics, Mon. Wea. Rev. (in press).

2. DESCRIPTION OF THE MODEL

2.1 Dynamic Equations

The NOAA model[3] is a 3D, hydrostatic, primitive equation model based, in part, on the Anthes and Warner[5] model. Finite difference approximations to the partial derivatives are second order and centered in both time and space. The model uses a staggered horizontal grid with variables $\Delta x = \Delta y = 5$ to 20 km over a 26×26 grid-point domain. Velocity components are defined at the cross points, while all other variables are defined at the dot points (see Figure 1). The use of the staggered grid leads to a smaller spatial truncation error of the pressure gradient term than in a non-staggered grid. In addition, boundary values of the velocity components do not appear in calculations of the continuity equation.[3,5] No map scale factor has been incorporated in this system of equations. There are 15 terrain-following computational levels in the vertical. The distribution of the computational levels was transformed from the conventional sigma coordinate

$$\sigma = (p - p_T)/\pi \quad , \tag{1}$$

where p is pressure, p_T is the pressure at the top of the model, and $\pi = (p_s - p_T)$, in which p_s is the surface pressure. When $p_T = 0$, $\sigma = p/p_s$. The transformation creates a vertical coordinate (ν) related to sigma by

$$\sigma = (4\nu - \nu^4)/3 \quad . \tag{2}$$

As shown in Table 1, the levels at which the vertical velocity ($\dot{\nu} = d\nu/dt$) is computed are staggered in the vertical with respect to the other variables in order to reduce the truncation error of the vertical finite differencing. The lower boundary is defined by a $5' \times 5'$ terrain data set archived at the Defense Mapping Agency and Aeronautics Center (DMAAC) in St. Louis, Mo.

The basic equations are expressed in flux form in the ν-coordinate system. The mass-weighted prognostic variables are

$$U = \pi u \quad ,$$

$$V = \pi v \quad ,$$

$$S = \pi s \quad , \text{ and}$$

$$W = \pi (q_v + q_{cw}) \quad , \tag{3}$$

---

5. Anthes, R.A., and Warner, T.T. (1978) Development of hydrodynamic models suitable for air pollution and other meteorological studies, Mon. Wea. Rev. 106:1045-1078.

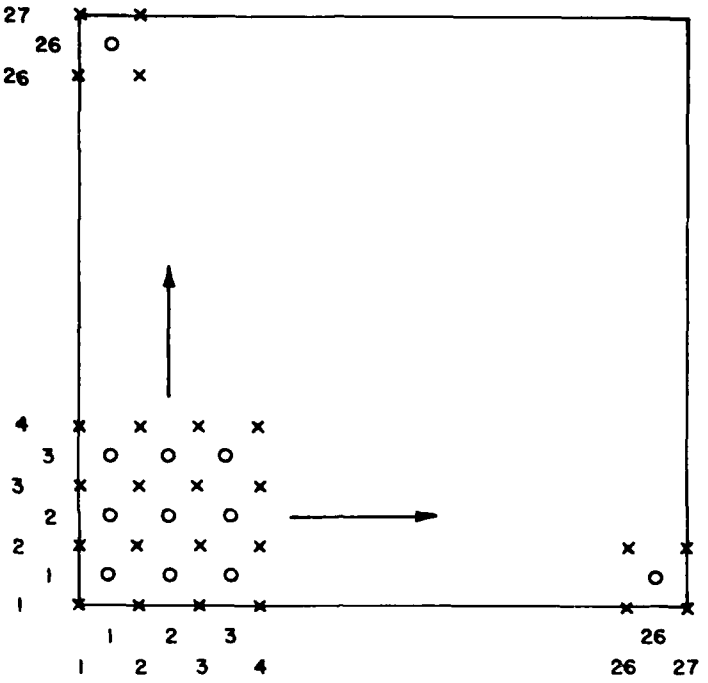

Figure 1. Staggered Horizontal Grid. Velocity components are defined on the 27 × 27 x-grid. All other variables are defined on the 26 × 26 o-grid

where S is the entropy (defined below), and q_v and q_{cw} represent the mixing ratios for water vapor and cloud water respectively. There are five predictive equations:

$$\frac{\partial U}{\partial t} = -\frac{\partial(Uu)}{\partial x} - \frac{\partial(Uv)}{\partial y} - \frac{1}{\sigma'}\frac{\partial(\sigma' U_{l'})}{\partial l'} + fV + \left(\phi - \frac{RT^*\sigma\pi}{P}\right)\frac{\partial \pi}{\partial x} - \frac{\partial(\pi\phi)}{\partial x} + F_u \tag{4}$$

$$\frac{\partial V}{\partial t} = -\frac{\partial(Vu)}{\partial x} - \frac{\partial(Vv)}{\partial y} - \frac{1}{\sigma'}\frac{\partial(\sigma' V_{l'})}{\partial l'} - fU + \left(\phi - \frac{RT^*\sigma\pi}{P}\right)\frac{\partial \pi}{\partial y} - \frac{\partial(\pi\phi)}{\partial y} + F_v \tag{5}$$

$$\frac{\partial S}{\partial t} = -\frac{\partial(Su)}{\partial x} - \frac{\partial(Sv)}{\partial y} - \frac{1}{\sigma'}\frac{\partial(\sigma' S_{l'})}{\partial l'} + F_s \tag{6}$$

$$\frac{\partial W}{\partial t} = -\frac{\partial(Wu)}{\partial x} - \frac{\partial(Wv)}{\partial y} - \frac{1}{\sigma'}\frac{\partial(\sigma' W_{l'})}{\partial \nu'} + F_w \tag{7}$$

$$\frac{\partial \pi}{\partial t} = -\int_0^1 \left(\frac{\partial U}{\partial x} + \frac{\partial V}{\partial y}\right)\sigma' dl' \quad . \tag{8}$$

Table 1. ν-Levels at a Gridpoint Over 325 m Terrain

Level	Pressure (mbar)	(m MSL)	Variables Defined
Top	0	Infinite	$d\nu/dt = 0$
1.0	44	21562	All Other Variables
1.5	87	-	$d\nu/dt$
2.0	131	14626	All Other Variables
2.5	175	-	...etc...
3.0	218	11448	
3.5	262	-	
4.0	305	9251	
4.5	348	-	
5.0	391	7509	
5.5	433	-	
6.0	475	6074	
6.5	516	-	
7.0	556	4871	
7.5	596	-	
8.0	635	3847	
8.5	672	-	
9.0	709	2971	
9.5	744	-	
10.0	777	2226	
10.5	809	-	
11.0	839	1609	
11.5	866	-	
12.0	892	1116	
12.5	914	-	
13.0	934	740	
13.5	951	-	
14.0	965	480	All Other Variables
14.5	975	-	$d\nu/dt$
15.0	981	343	All Other Variables
Bottom	983	325	$d\nu/dt = 0$

The friction/diffusion terms (F_u, F_v, F_s, and F_w) will be explained in Section 2.2. Three diagnostic equations provide information for the prognostic equations:

$$\dot{\nu} = \frac{1}{\pi\sigma'}\int_0^{\nu} \sigma' \left(\frac{\partial \pi}{\partial t} + \frac{\partial U}{\partial x} + \frac{\partial V}{\partial y}\right) d\nu \quad , \tag{9}$$

$$\frac{\partial \phi}{\partial \pi} = - C_p \Theta(1 + 0.61\, q_v) \quad , \text{ and} \tag{10a}$$

$$S = \pi[\ln(T/P) + Lq_v/C_pT] \quad . \tag{10b}$$

The following definitions apply:

$$\sigma' = d\sigma/d\nu \qquad \phi = gz$$
$$\dot{\nu} = d\nu/dt \qquad T^* = T(1 + 0.61\, q_v)$$
$$\hat{P} = (P/P_o)^{R/C_p} \qquad L = 597.3 - 0.566\,(T - 273.16)$$
$$\theta = T/\hat{P} \quad .$$

The saturation vapor pressure with respect to water, e_s, is taken from Murray:[6]

$$e_s = 6.11 \exp\,[17.27\,(T - 273.16)/(T - 35.86)] \quad . \tag{11}$$

In order to determine the temperature and moisture variables, the model first computes T_s (saturation temperature) and q_{vs} (saturation mixing ratio). If the air is saturated ($W > \pi q_{vs}$), the mixing ratio is a known function of temperature, and Eq. (10b) becomes a transcendental equation for the temperature, T_s, corresponding to saturation with respect to liquid water. If, on the other hand, the air is unsaturated ($W \leq \pi q_{vs}$), the mixing ratio in Eq. (10b) is replaced by W/π and the temperature is solved for directly. The finite difference forms of Eqs. (4) through (10) are given by Nickerson.[3]

2.2 Numerical Methods and Physical Parameterizations

A time step of between 10 and 30 sec may be used in this model. Two different procedures have been developed to control the small scale, high frequency waves generated by the model. The first uses the Matsuno Time-and-Space-Uncentered (TASU)[7] procedure in combination with a five-point spatial smoother

6. Murray, F.W. (1967) On the computation of saturation vapor pressure, J. Appl. Meteorol. 6:203-204.

7. Arakawa, A., and Mintz, Y. (1974) The UCLA general circulation model, Notes from the workshop. 25 March - 4 April 1974, Department of Meteorology, UCLA.

applied to the forecast winds on ν-surfaces at each time step. The TASU procedure requires that two time steps (each ninth and tenth) be broken up into four half-time steps. Unfortunately, the five-point operator has been shown[8] to remove energy from the meteorologically significant gravity-inertia (GI) wave modes (as well as the non-meteorological GI wave modes) generated during the geostrophic adjustment process. The other time-and-space smoothing procedure uses an Asselin filter[9] in conjunction with explicit, fourth-order horizontal diffusion terms within the momentum equations. The Asselin filter produces somewhat smoother time integrations without the need for extra half-time steps as in the TASU scheme. However, the latter requires a shorter time step in order to maintain computational stability; thus, the overall computation time is increased (by about 20 percent in recent tests). The diffusion terms F_u and F_v in Eqs. (4) and (5) serve two purposes: the first is to control energy growth over certain spatial scales in the model domain; the second is to represent the diffusion processes that actually occur in the real atmosphere.

At the top boundary, $\dot{\nu} = 0$. An upper absorbing layer[2] or "sponge" was developed and tested.[4] This layer permits certain vertically-propagating GI waves (generated by various local forcing mechanisms) to exit the model domain.

As stated in the introduction, one of the most difficult problems with limited-area models is the proper treatment of the variables at the lateral boundaries. This, in turn, greatly affects the accuracy of solutions on the interior of the domain. Except for outflow winds extrapolated outward from interior values, the NOAA model originally used time-invariant lateral boundary conditions. Recently, Nickerson[4] incorporated an Orlanski radiation boundary condition[10] for the lateral boundaries.

The model treats the first vertical computational layer between the lower boundary and the first grid point above the surface (approximately 18 m thick) with the Businger-Dyer formulation[3,11] for a constant-flux surface layer. This formulation expresses the friction velocity and surface fluxes of sensible and latent heat as non-dimensional functions (F and G) of height and the Monin-Obukov length. Which particular set of equations is used depends on whether the surface layer is unstable, mildly stable, or stable.

---

8. Seitter, K.L. (1984) personal correspondence.

9. Asselin, R.A. (1972) Frequency filter for time integrations, Mon. Wea. Rev. 100:487-490.

10. Orlanski, I. (1976) A simple boundary condition for unbounded hyperbolic flows, J. Comp. Phys. 21:251-269.

11. Nickerson, E.C., and Smiley, V.E. (1975) Surface layer and energy budget parameterizations for mesoscale models, J. Appl. Meteorol. 14:297-300.

A boundary layer is defined between the first grid point above the surface (Z_B = 18 m) and the layer (Z_A = 1000 m), and eddy exchange coefficients are computed in accordance with the profile given by O'Brien.[12] Between Z_A and Z_B, separate coefficients are computed for momentum (K_u) and for temperature and moisture (K_T) by equations analogous to

$$K(Z) = K(Z_A) + (Z - Z_A)^2/(\Delta Z)^2 \left(K(Z_B) - K(Z_A) + (Z - Z_B) \{K'(Z_B) + 2[K(Z_B) - K(Z_B)]/\Delta Z\} \right) . \quad (12)$$

Also,

$$\left.\begin{aligned} K_u(Z) &= u^*/F'(Z) \\ K_T(Z) &= u^*/G'(Z) \end{aligned}\right\} \quad \text{at } Z = Z_B, \text{ and}$$

$$\left.\begin{aligned} K_u(Z) &= 0 \\ K_T(Z) &= 0 \end{aligned}\right\} \quad \text{for } Z > Z_A \quad (13)$$

where u^* is the friction velocity, the prime denotes the derivative with respect to Z, and $\Delta Z = (Z_A - Z_B)$. The friction terms in Eqs. (4) through (7) are written as:

$$F_u = A \frac{\partial}{\partial \nu} \left(AK(u) \frac{\partial U}{\partial \nu} \right) ,$$

$$F_v = A \frac{\partial}{\partial \nu} \left(AK(u) \frac{\partial V}{\partial \nu} \right) ,$$

$$F_s = A \frac{\partial}{\partial \nu} \left(AK(T) \frac{\partial S}{\partial \nu} \right) , \quad \text{and}$$

$$F_w = A \frac{\partial}{\partial \nu} \left(AK(T) \frac{\partial W}{\partial \nu} \right) , \quad (14a)$$

where $A = -gp/RT\pi\sigma'$. At the lower boundary ($\nu = \sigma = 1$),

12. O'Brien, J.J. (1970) On the vertical structure of the eddy exchange coefficient in the planetary boundary layer, J. Atmos. Sci. 27:1213-1215.

$$AK(u)\frac{\partial u}{\partial \nu} = \pi u_*^2 \cos^2 \quad ,$$

$$AK(u)\frac{\partial v}{\partial \nu} = \pi u_*^2 \sin^2 \quad ,$$

$$AK(T)\frac{\partial S}{\partial \nu} = \pi\left(\frac{Q_s P}{T} + \frac{LQ_e}{C_p}\right) \quad , \text{ and}$$

$$AK(T)\frac{\partial W}{\partial \nu} = \pi Q_e \quad , \tag{14b}$$

where $\tan\alpha = V_h/U_h$ (the ratio of the two wind components at the first grid point above the surface), and the surface fluxes of heat and moisture (Q_s and Q_e) are given by

$$\pi Q_s = (\theta_o - \theta_h)\sqrt{U_h^2 + V_h^2}/FG \quad , \text{ and}$$

$$\pi Q_e = (q_o - q_h)\sqrt{U_h^2 + V_h^2}/FG \quad . \tag{14c}$$

The NOAA model employs detailed microphysical parameterizations of warm rain processes (the "warm" version)[13] and frozen precipitation processes (the "cold" version).[14] The warm version begins with a forecast of W and an existing rain water mass with a log-normal drop size distribution. Raindrops do not grow by diffusion, but may form and disappear by separate processes of evaporation, advection, sedimentation, raindrop self-collection, and cloud drop accretion. In order to keep track of the effect of these processes, the model carries two rain descriptors at each grid point: the rain water mixing ratio and the raindrop specific number concentration. The cold version additionally forecasts three types of ice particles: unrimed, partially rimed, and graupel. Therefore, six precipitation variables are necessary at each grid point, namely, mixing ratio and number concentration for each of the three ice particle types. These particles are assumed to exhibit a Marshall-Palmer size distribution. Physical processes

---

13. Nickerson, E. C., and Richard, E. (1982) On the distribution and evolution of clouds and rain over the Vosges and Black Forest mountains: a three-dimensional mesoscale simulation with parameterized microphysics, in Preprints of the 5th Conference on Numerical Weather Prediction, American Meteorological Society, Boston, pp. 223-227.

14. Nickerson, E. C., Smith, D. R., Magaziner, E. L., and Chappell, C. F. (1979) A numerical simulation of snowfall over rugged mountainous terrain, in Preprints of the 4th Conference on Numerical Weather Prediction, American Meteorological Society, Boston, pp. 260-265.

in the cold model include advection, sedimentation, spontaneous nucleation of unrimed crystals, accretion of ice particles, deposition/sublimation, and transfer of growing ice particles to the next larger category. In both the warm and cold versions, precipitation that falls through the lowest computational level accumulates on the ground.

The model has no parameterizations for radiative surface heating and cooling, sub-grid scale convection, or surface characteristics such as vegetation and soil moisture. Surface temperature and moisture are maintained constant in time.

2.3 Model Initialization

A description of the initialization procedure of the model is given here to help better understand several problems that are noted in Section 3.

First, the model computes surface pressure at each grid point from

$$p_s = p_o \left(\frac{T_v + Z_T \gamma_s}{T_v} \right)^{g/R_d \gamma_d} , \tag{15}$$

where p_s is the surface pressure, p_o the gridded value of sea level pressure, Z_T the terrain elevation, and T_v an assumed mean virtual temperature. A standard lapse rate is assumed ($\gamma_s = 0.0065°K/m$), and g, R_d, and γ_d are gravitational acceleration, the gas constant for dry air, and the dry adiabatic lapse rate, respectively. The winds, temperature, and moisture are initialized from a single radiosonde located at the grid center. The model computes pressure at each grid point on the constant ν-surfaces. The pressure on each ν-surface is a constant multiple of the underlying surface pressure. Then, temperatures and mixing ratios are determined at each ν-surface from a linear-in-pressure vertical interpolation of the sounding data. An unfortunate consequence of the single-sounding initialization is that, on a given ν-surface, horizontal gradients of temperature and moisture arise solely from the existence of underlying gradients of surface elevation. The model insures that the temperature at the first ν-level above ground (level 15) is less than the ground temperature (level 16). Then, the hypsometric equation [Eq. (10a)] is integrated upward from the surface to determine geopotential, without direct reference to the sounding. As a result, the horizontal continuity of geopotential on ν-surfaces is also affected by the underlying gradients of surface elevation. Finally, the u- and v-wind components are similarly interpolated from the sounding to the ν-surfaces. All other model variables (e.g., entropy) are computed from these gridded variables.

The model is initialized with wind fields out of dynamic balance with the mass distribution. Previous tests by Nickerson and others have suggested that an elapsed time of one model-hour is needed for the mutual adjustment of these fields.

2.4 Model Configurations Under Development

At this time, there are two different versions of the model under development. The first is the AFGL/NOAA Mesoscale Model, described in Table 2. The model is written in ANSI FORTRAN 77. It requires 70,592 decimal words of central memory, which economizes on large-core-memory requirements at the expense of run time. In this version, the numerous $26 \times 26 \times 16$ point variable arrays generally reside in mass storage. One vertical east-west plane is buffered into core at a time; hence, there is never more than about 15 percent of the data in core at once. Run time for a 7-h integration with 30-sec time steps on the CDC Cyber 170/750 includes 200 min central processing time and 790 min input/output time.

Table 2. Features of the AFGL/NOAA Model and the NOAA/LAMP Model

Feature	AFGL/NOAA	NOAA/LAMP
Microphysics	Warm or Cold	Cold
Time Integration	Centered Differences	Centered Differences
Time/Space Smoothing	Matsuno TASU/5-Point Smoother	Asselin/Explicit Diffusion
Upper Boundary Conditions	Constant (Reflective)	Sponge or Constant
Lateral Boundary Conditions	Time-Invariant/Extrapolate Outflow Wind	Orlanski Radiative
Vertical Levels	15	15 (31 in the 2D Version)
Computer Use Strategy	15 Percent Core, 85 Percent Mass Storage	Fully Core-Resident
Computer	CDC Cyber 170/750	Cray 1

The second version is under development at NOAA/ERL and in France by cooperative agreement with the Laboratoire Associe de Meteorologie Physique (LAMP) at Clermont. The NOAA/LAMP model is described in Table 2. It is frequently useful to test numerical aspects of a model, such as vertical resolution or the parameterization of physical processes, with a less complex and more

efficient 2D analog to the 3D model. Most of the above features are also present in a 2D (x-z) version of the NOAA/LAMP model.

3. RESULTS OF A BASELINE TEST

While the primary objective during the first year of the AFGL program was to perform a baseline test of the NOAA 3D model, three secondary achievements were also accomplished. First, the model was adapted to the AFGL computer (hence the name AFGL/NOAA model). The warm version was selected for the baseline test. Second, a baseline data set was selected and prepared. A single vertical sounding was used to initialize the model variables; however, the baseline data set also contains a dense, 3-hourly radiosonde set (27 March 1982), along with surface, rain gauge, and satellite data. Third, it was necessary to write software that processed the model output into graphical and statistical form[15] for later verification against the baseline data.

The baseline test revealed several major problems with the model. These problems appeared to stem from the initialization and the lateral boundary conditions in large part, and they disrupted the forecast to the point where it was not possible to assess the performance of other parts of the program (e.g., boundary layer formulation and rain microphysics).

The initialization described in Section 2.3 was found to be far from adequate in three respects. First, the resulting model analyses of temperature, moisture, and winds have no realistic horizontal gradients on the computational surfaces. Using the analyzed temperatures in the vertical integration of the hydrostatic equation yields geopotential-height fields for which the contours are roughly parallel to contours of terrain height. For example, notice the discrepancy at 500 mbar between the observed heights (Figure 2) and the corresponding single-sounding initialized heights (Figure 3): the direction of the gradient is completely reversed. Second, the temperature analysis at the lowest level is not representative of the mean surface and boundary layer conditions. Third, the period of the initial geostrophic adjustment process was excessively long.

Two approaches are under development at NOAA/ERL and AFGL to improve the initialization scheme. They are: (1) revision of the single-sounding technique by imposing a variational constraint on the wind and mass fields, with sensitivity to boundary layer structure; and (2) the use of more initial data (e.g., multiple

---

15. Seitter, K. L. (1984) A three-dimensional radiation boundary condition for mesoscale numerical models, Final Report on 1984 USAF-SCEEE Summer Faculty Research Program, Contract No. F49620-82-C-0035.

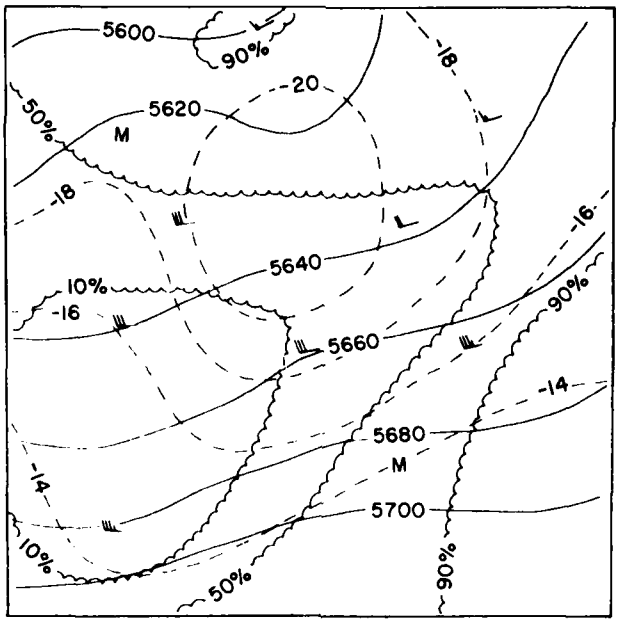

Figure 2. 500 mbar Mesoscale Analysis at 1200 GMT, 27 Mar 82. Height (solid), temperature (dashed), relative humidity (scalloped), and wind (m/sec). Stations marked M reported temperature and humidity, but not wind

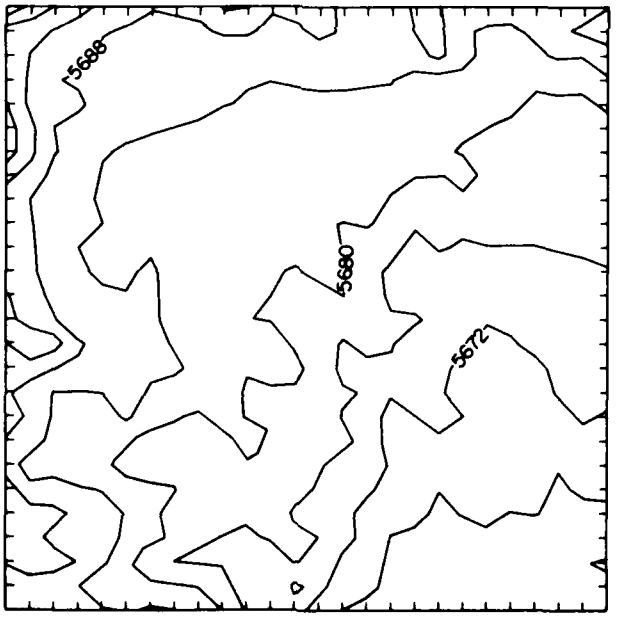

Figure 3. Initial 500 mbar Height (m)

soundings, surface data, or output from a larger model). Some simple experiments for improving the model initialization in the lower layers using surface data will be discussed in Appendix A.

As mentioned above, a major problem noted in the baseline test was the persistent imbalance between wind and mass fields during the forecasts. The 3-h forecast of a 500 mbar height field shown in Figure 4 normally implies a north-easterly geostrophic wind; yet, the corresponding forecast wind direction in Figure 5 is westerly to north-westerly. The forecast shows little evidence of geostrophic balance after 3 h of integration. It appears that the only practical solution to this dynamic imbalance problem is to begin with a more realistic, or balanced, initialization.

Most of the forecast fields (with the exception of wind, which was specifically smoothed at each time step) exhibited significant $2\Delta x$ noise. These waves did not appear very large in amplitude (see Figure 4). Waves in the 500 mbar temperature field (not illustrated) were about 1°C in amplitude. The wave pattern appeared to originate near the eastern (downwind) boundary and propagate toward the center of the domain during the forecast. In addition, a gradually amplifying disturbance was fixed along the western boundary. This evidence strongly suggests that these waves probably arose from inadequate numerical treatment of the

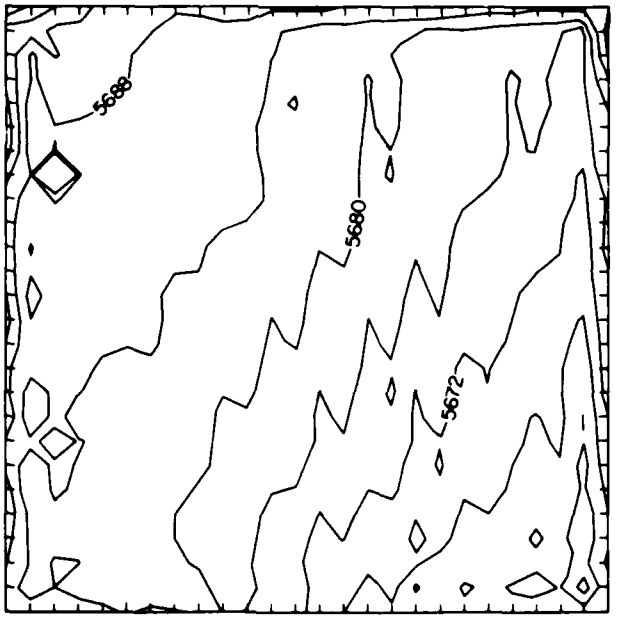

Figure 4. Three-Hour Forecast of 500 mbar Height (m)

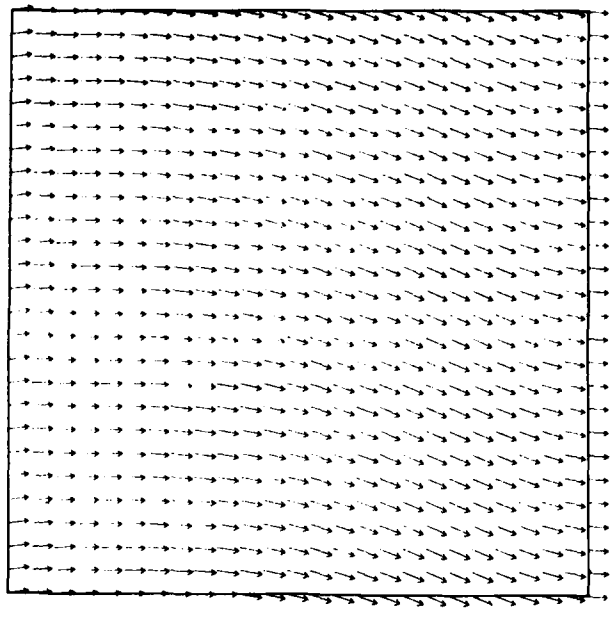

Figure 5. Three-Hour Forecast of 500 mbar Wind. Longest vector represents 33 $msec^{-1}$ (baseline model winds were initially uniform west-southwest)

lateral boundaries. Figure 6 illustrates the sea level pressure forecast. Surface pressure is maintained constant in time at the lateral boundaries, but may vary in the interior. Notice the $2\Delta x$ noise in this field at the west and east boundaries. One variable that reacted strongly to this was the vertical velocity, w (Figure 7), which had an upward maximum of 12 cm sec^{-1} near the eastern edge and an even stronger downward region on the western edge. Note the corresponding precipitation maximum along the north and east edges (Figure 8).

The boundary condition problem is likely to be solved only with a more complex numerical treatment. This was determined after the model continued to exhibit excessive GI-wave activity even after it was initialized with the actual AVE/VAS "truth" data. In this experiment, the four model input fields of θ, q_v, u, and v were objectively analyzed to the model grid points (see Figure 9). No balancing of the mass and momentum fields was performed. The model was then run for five hours, and output fields were compared with the previously discussed model run. While the result of this latter initialization may be viewed as a significant improvement from the single-sounding case, Figure 10 (500 mbar geopotential height in m) shows that large GI waves continue to dominate the numerical solution. Higher frequency noise also continues to be a problem near the boundaries, suggesting that the time-invariant boundary conditions may be a source of much GI energy generation.

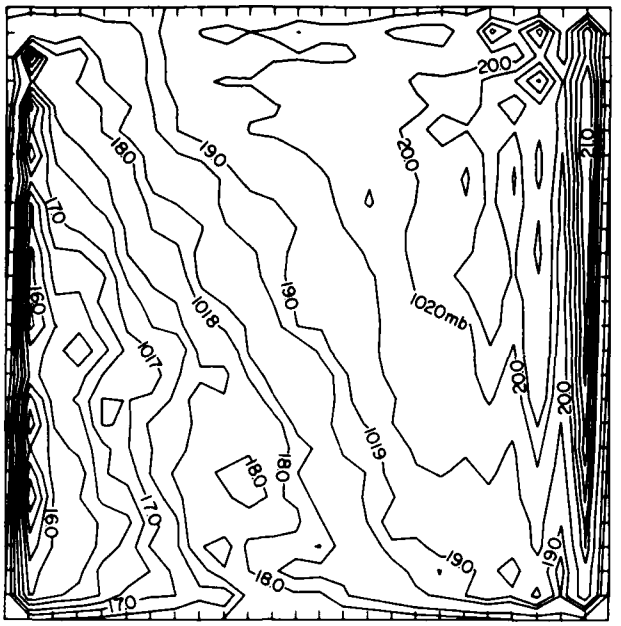

Figure 6. Three-Hour Forecast of Sea-Level Pressure (mbar). Isobars at 0.25 mbar intervals

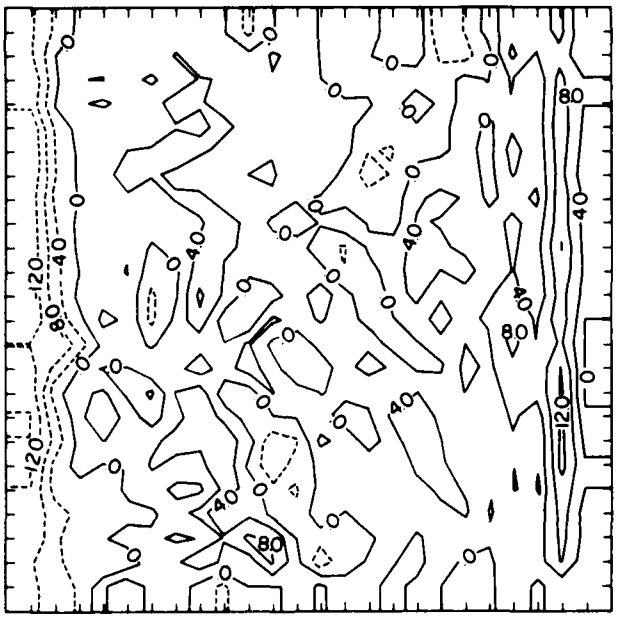

Figure 7. Three-Hour Forecast of Vertical Velocity (cm sec^{-1}). Solid lines are upward, dashed lines are downward

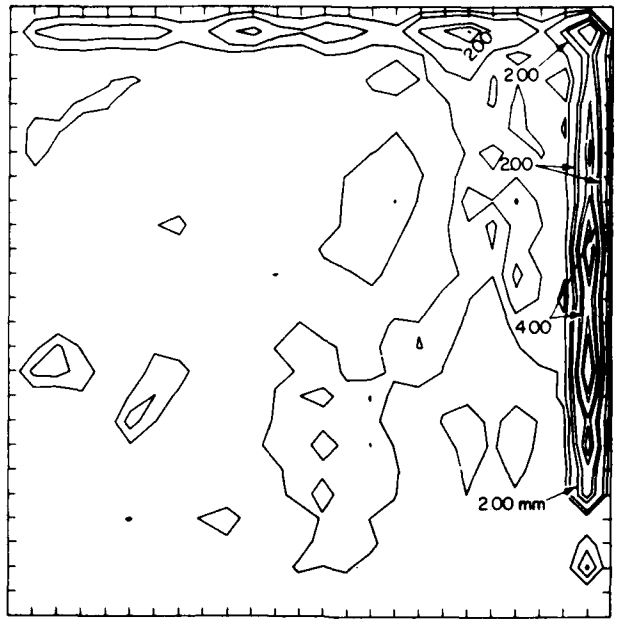

Figure 8. Three-Hour Forecast of Total Precipitation (mm). Contours at 0.5 mm intervals

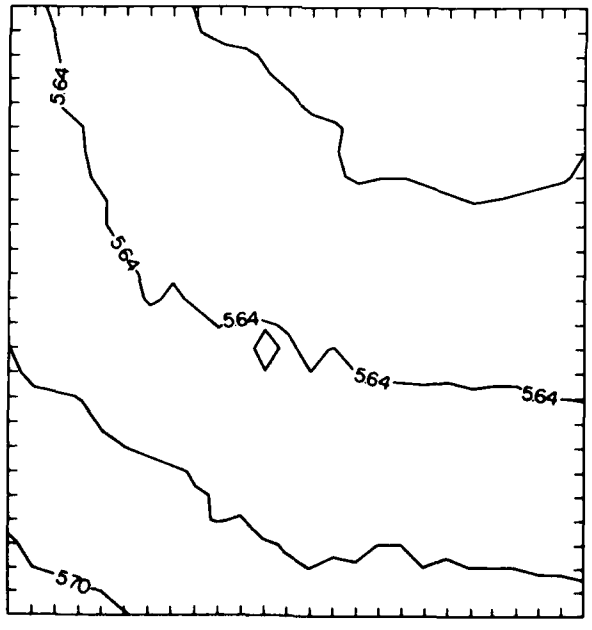

Figure 9. Initial 500 mbar Height (m): From AVE/VAS Data Set

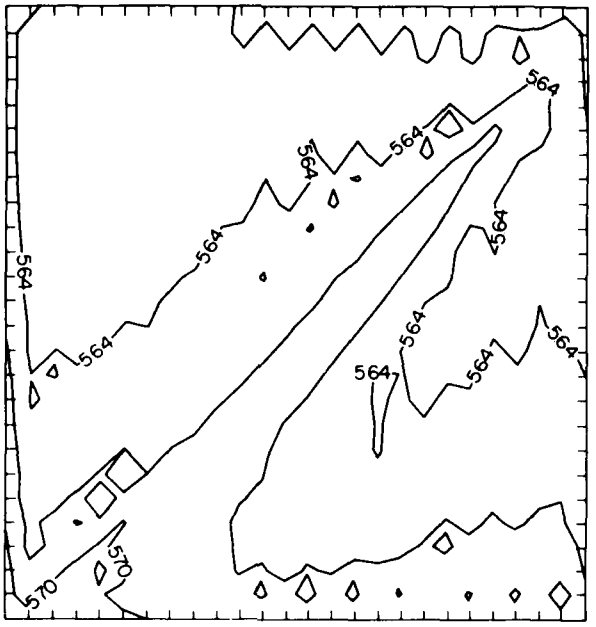

Figure 10. Five-Hour Forecast of 500 mbar Height (m)

4. CONCLUSIONS

A numerical mesoscale forecast model was selected for potential use by the Air Force in an operational mode, either in a nested configuration, or as a stand-alone model in a base-weather station. This NOAA model and many of its numerical and meteorological features were described in this report. Two versions were specified: the first is under development at NOAA/ERL (the NOAA/LAMP Model), and the other is under development at AFGL (the AFGL/NOAA Model).

A baseline test of the model revealed several problems. The initialization scheme computed initial fields of mass and momentum that failed to mutually adjust after several hours of integration. Work is under way at AFGL and at ERL to improve this initialization; subsequent techniques designed to improve the initial conditions appeared to be a step in the right direction. The nonmeteorological GI wave noise evident in most of the forecast fields appeared to result from poor treatment of the variables at the lateral boundaries.

References

1. Air Weather Service (1984) Capabilities Master Plan (CMP) 1984-1985, Headquarters AWS, Scott AFB, Ill.
2. Anthes, R.A. (1983) Regional models of the atmosphere in middle latitudes, Mon. Wea. Rev. III:1306-1335.
3. Nickerson, E.C. (1979) On the numerical simulation of airflow and clouds over mountainous terrain, Beit. zur Physik der Atmos. 52:161-177.
4. Nickerson, E.C., Richard, E., Rosset, R., and Smith, D. (1985) On the numerical simulation of clouds, rain, and airflow over the Vosges and Black Forest Mountains: A meso-β model with parameterized microphysics, Mon. Wea. Rev. (in press).
5. Anthes, R.A., and Warner, T.T. (1978) Development of hydrodynamic models suitable for air pollution and other meteorological studies, Mon. Wea. Rev. 106:1045-1078.
6. Murray, F.W. (1967) On the computation of saturation vapor pressure, J. Appl. Meteorol. 6:203-204.
7. Arakawa, A., and Mintz, Y. (1974) The UCLA general circulation model, Notes from the workshop, 25 March - 4 April 1974, Department of Meteorology, UCLA.
8. Seitter, K.L. (1984) personal correspondence.
9. Asselin, R.A. (1972) Frequency filter for time integrations, Mon. Wea. Rev. 100:487-490.
10. Orlanski, I. (1976) A simple boundary condition for unbounded hyperbolic flows, J. Comp. Phys. 21:251-269.
11. Nickerson, E.C., and Smiley, V.E. (1975) Surface layer and energy budget parameterizations for mesoscale models, J. Appl. Meteorol. 14:297-300.
12. O'Brien, J.J. (1970) On the vertical structure of the eddy exchange coefficient in the planetary boundary layer, J. Atmos. Sci. 27:1213-1215.

13. Nickerson, E. C., and Richard, E. (1982) On the distribution and evolution of clouds and rain over the Vosges and Black Forest mountains: a three-dimensional mesoscale simulation with parameterized microphysics, in Preprints of the 5th Conference on Numerical Weather Prediction, American Meteorological Society, Boston, pp. 223-227.

14. Nickerson, E. C., Smith, D. R., Magaziner, E. L., and Chappell, C. F. (1979) A numerical simulation of snowfall over rugged mountainous terrain, in Preprints of the 4th Conference on Numerical Weather Prediction, American Meteorological Society, Boston, pp. 260-265.

15. Seitter, K. L. (1984) A three-dimensional radiation boundary condition for mesoscale numerical models, Final Report on 1984 USAF-SCEEE Summer Faculty Research Program, Contract No. F49620-82-C-0035.

Appendix A

Alternative Boundary Layer Initialization Techniques

Initializing a mesoscale model with available conventional surface and upper-air data can be a difficult problem. Sufficient surface observations are generally available to obtain a good set of initial surface analyses. However, upper-air observations are nearly always far too sparse to describe the details of atmospheric structure, especially in the boundary layer. The AFGL mesoscale model, with 20-*km* horizontal resolution, encompasses a 500 × 500 km area. Within this area, there are in excess of 25 surface stations, but only one upper-air station. This distribution of observations, which is typical across the United States, suggests that radiosonde data may be supplemented with data extracted from the surface so that sufficient detail can be obtained to accurately initialize a mesoscale model.

The current version of the AFGL mesoscale model uses a single sounding to initialize model fields at all levels over the entire model domain. This has been shown to be relatively successful in certain situations where local terrain forcing dominates the atmospheric flow. However, in regions where terrain forcing is less, the initial horizontal fields generated by the single-sounding model initialization tend to reflect the terrain rather than the actual distribution of atmospheric parameters. These single-sounding model-initialized fields, therefore, are physically unrealistic, and, consequently, a model initialized with these fields is unlikely to generate useful forecasts.

As a first attempt to improve the initialization of the AFGL mesoscale model, several simple techniques, using the relatively dense surface observations in conjunction with the current single-sounding model initialization scheme, were

developed to generate a "blended" initialization for the lower model levels. The idea was that the detail and realism of the lower atmospheric fields used to initialize the model could be greatly enhanced by the valuable information contained in the surface analysis. The blended fields were calculated for model levels 15, 14, 13, 12, and 11, approximately corresponding to pressure levels of 998, 981, 950, 907, and 853 mbar, respectively. These model levels were chosen, because analyzed horizontal fields of quantities generally resemble surface fields.

The fields necessary to initialize the model are potential temperature, specific humidity, and the U and V components of the horizontal wind. The initial fields generated by the blending technique and the single-sounding model initialization fields were then compared to a "truth set" of analyzed radiosonde observations. The truth data set was generated from a network of 21 densely spaced AVE/VAS and National Weather Service radiosonde sites located in Texas and Oklahoma. The truth data set, available at 25-mbar intervals, was interpolated to the model ν-levels. The model ν-level data was then analyzed to a 17×16 (1/2 deg) grid using a 2-pass Barnes analysis routine. The 1/2 deg data was then horizontally interpolated to the smaller 26×26 20-km model grid.

The truth data set was then compared, grid point by grid point, to the single-sounding model initialization fields. Root-Mean-Square Error (RMSE) and Mean Absolute Error (MAE) statistics were computed for each parameter, at each ν-level. These error statistics were then used as the basis in comparing the improvement (or lack of improvement) of the blending techniques to the single-sounding model initialization. Five tests were performed, and each is briefly described in the following paragraphs.

Test I was designed to blend the surface fields with the single-sounding model initialization such that the blended fields would be composed of 100 percent surface data at the model surface (ν-level 16), and would decrease according to a mass-weighted distribution to 0 percent surface data and 100 percent single-sounding model initialization at ν-level 10. The weights for each level are shown in Table A1. This would allow the surface analysis to influence the initial model fields up to approximately the 850 mbar level.

Table A1. Blended-Initialization Weights for Test I

	ν-15	ν-14	ν-13	ν-12	ν-11
Surface	0.99	0.91	0.75	0.54	0.26
Single-Sounding	0.01	0.09	0.25	0.46	0.74

Test II was designed to measure the effect of increasing the weight given to the surface analysis. The weights were chosen to be strictly mass weighted, assuming a surface pressure of approximately 1000 mbar. The weights for each level are shown in Table A2.

Table A2. Blended-Initialization Weights for Test II

	ν-15	ν-14	ν-13	ν-12	ν-11
Surface	0.998	0.981	0.950	0.907	0.853
Single-Sounding	0.002	0.019	0.050	0.093	0 147

Test III was designed simply to show the effect of ignoring the single-sounding model initialization by applying the actual surface fields at the tested model levels. Thus, the analyzed surface fields were given a weight of 1.00, and the single-sounding model initialization fields were given a weight of 0.00, both at all ν-levels.

Test IV was designed to incorporate the vertical distribution of each parameter observed from the single sounding with the analyzed surface fields. The lapse rate of each parameter was calculated from the single sounding. The lapse rate of each parameter was then applied to the analyzed surface fields to calculate blended fields for each parameter at each ν-level.

Test V was an attempt to improve upon the other tests, all of which failed to generate accurate blended wind fields, and, thus, was applied to U and V fields only. An Ekman layer was assumed, and the horizontal wind components were calculated for each ν-level and blended with the single-sounding model initialization horizontal wind components with the same weights as in Test I.

Table A3 indicates that Test I and Test IV provide significant improvement over the single-sounding model initialization fields for potential temperature and mixing ratio at all levels. Test IV shows the most improvement overall, exhibiting the smallest errors at the higher levels of all tests. It shows improvements for potential temperature of 77, 77, 71, 55, and 53 percent over the single-sounding model initialization for ν-levels 15, 14, 13, 12, and 11, respectively, and improvements of 69, 65, 41, 39, and 57 percent at the same ν-levels for mixing ratio. Tests II and III also show considerable improvement over the single-sounding model initialization for potential temperature and mixing ratio at ν-levels 15, 14, and 13; however, at ν-levels 12 and 11, these methods do poorly due to the large weights given to the surface analysis.

Table A3. Root-Mean-Square Errors of Blended Sounding Technique

Theta (°K)						
ν-Level	Single-Sounding	I	II	III	IV	V
15	2.78	0.68	0.69	0.69	0.69	-
14	2.93	0.69	0.70	0.72	0.70	-
13	2.27	0.68	1.03	1.16	0.81	-
12	2.39	1.92	3.35	3.78	1.18	-
11	3.14	2.29	7.43	8.98	1.90	-
MIXR (gkg^{-1})						
15	1.21	0.36	0.37	0.37	0.37	-
14	1.02	0.36	0.36	0.38	0.35	-
13	0.70	0.57	0.65	0.67	0.39	-
12	0.81	0.65	0.70	0.74	0.49	-
11	0.82	0.71	0.57	0.56	0.35	-
u ($msec^{-1}$)						
15	2.82	1.75	1.76	1.77	1.72	6.25
14	4.13	3.56	3.68	3.71	2.66	14.67
13	4.43	4.24	4.84	5.02	3.47	17.66
12	3.37	3.95	4.99	5.30	5.28	11.33
11	4.08	4.46	7.88	8.94	6.68	4.74
v ($msec^{-1}$)						
15	1.85	1.24	1.25	1.25	1.25	0.90
14	0.85	2.29	2.46	2.51	2.48	3.36
13	1.16	4.04	4.04	5.13	4.93	7.80
12	1.75	5.08	5.08	8.63	7.95	9.87
11	4.82	2.37	2.37	8.33	8.47	2.76

While these blending techniques show great potential for improvement of model initial analyses over the single-sounding model initialization technique for potential temperature and mixing ratio, the results for the horizontal wind components are quite poor. Table A3 shows some improvement over the single-sounding model initialization in the lowest layers; however, the errors for all techniques tend to increase with height and are generally worse than the single-sounding model initialization. Each technique crudely allows a turning of the wind with height by including both a weighted surface wind and a weighted single-sounding model initialized wind in the U and V calculations, or by the lapse rate or Ekman spiral techniques. They all ignore stability, terrain, and local effects, however, and Tests I-IV assume that the one sounding used in the single-sounding model initialization is representative of the entire model domain.

The results of these tests are based on only one case, and, although they show the potential for significant improvement over the single-sounding model initialization for potential temperature and mixing ratio, they are not conclusive. Future tests will be conducted using analyses of three or more radiosonde observations from the area surrounding the model domain. The radiosonde observations will be from the conventional network of radiosonde sites, and, thus, typical of day-to-day conditions. Interpolating these analyses to the smaller model grid will yield a more realistic representation of the atmosphere than the single-sounding model initializations, with reasonable gradients. These more realistic analyses will then be blended with the surface analyses as in Tests I-IV. More sophisticated blending techniques must be developed to improve the U and V initialization fields.

END

DTIC

5-86